Journal of Alloys and Compounds 509 (2011) 6267–6272

Contents lists available at ScienceDirect

Journal of Alloys and Compounds

journal homepage: www.elsevier.com/locate/jallcom

Corrosion behavior of Ti–Mo alloys cold rolled and heat treated

Ying-Long Zhou [a,*], Dong-Mei Luo [b]

[a] Department of Mechatronics Engineering, Foshan University, 18 Jiangwan Yi Rd, Foshan 528000, Guangdong Province, PR China
[b] Department of Civil Engineering, Foshan University, 18 Jiangwan Yi Rd, Foshan 528000, Guangdong Province, PR China

ARTICLE INFO

Article history:
Received 28 December 2010
Received in revised form 28 February 2011
Accepted 6 March 2011
Available online 11 March 2011

Keywords:
Ti–Mo alloy
XPS
Oxide film
Corrosion resistance
Metallic biomaterial

ABSTRACT

Corrosion behavior of (α + β) Ti–10Mo and β Ti–20Mo (mass%) alloys cold rolled and solution heat treated was investigated by studying the anodic polarization curves at 310 K in 5 mol% HCl solution to determine the potential use of those alloys in biomedical applications. The anodic films formed on the surfaces of the alloys were examined using X-ray photoelectron spectroscopy analysis and scanning electron microscopy. The results reveal that both of the Ti–Mo alloys cold rolled and solution treated exhibit a passive behavior in 5% HCl solution, which is attributed to the passive film formation of a mixture of MoO_3 and TiO_2. The cold rolling process does not influence the formation of passive films on the Ti–Mo alloys although it slightly increases the passive current densities. The corrosion resistance of the Ti–Mo alloys increases with Mo content and both of the Ti–Mo alloys exhibit better corrosion resistance than commercial pure Ti—the currently used metallic biomaterial.

1. Introduction

Recently, there has been a tread towards the development of β type Ti alloys to replace the conventional metallic biomaterials such as stainless steel, Co–Cr alloys, pure Ti and Ti–6Al–4V alloy, especially for orthopedic implant applications since the β phase in Ti alloys exhibits a significantly lower modulus and the β Ti alloys satisfy most of the other requirement for ideal metallic biomaterials [1–3]. Many new β Ti alloys composed of non-toxic and non-allergic elements such as Nb, Ta, Zr, Hf, Mo, and Sn have been studied for biomedical applications [1–9].

Among the above safe alloying elements, Nb, Ta, and Mo are considered as the excellent β-phase stabilizers for Ti alloys used for biomedical applications [1–6]. An increase in alloying content of those β phase stabilizers usually tends to stabilize the β phase and decrease the elastic modulus of the Ti alloys. On the other hand, however, Nb, Mo, and Ta belong to refractory elements with very high melting points (2750, 2896, and 3290 K for Nb, Mo, and Ta, respectively) [10] and heavy densities (8.57, 10.28, and 16.65 g/cm^3 for Nb, Mo, and Ta, respectively) [10]. Therefore, an increase in their alloying contents leads to both higher melting points and heavier densities of obtained β Ti alloys, which is undesirable for biomedical applications since a biomedical Ti-base alloy should have (1) a reasonably low density; (2) little or no cytotoxic metals in its composition; (3) a high strength and long fatigue life; (4) a low elastic modulus comparable with that of cortical bone; (5) a large room-temperature plasticity so that it can be easily formed; and (6) good casting properties so that it can be easily cast into defect-free materials [11]. Combining with the above two viewpoints, it can be expected that the β Ti alloys with the lowest alloying content of the above β stabilizers is desirable for biomedical applications because they have a good combination of low elastic modulus, low melting point, and low density. In other words, the most effective β-phase stabilizer is preferable for the Ti biomaterials.

The concentrations of alloying elements, Mo, Nb, and Ta above which β is retained after quenching from β field are 8, 22, and 52 mass%, respectively for binary Ti–Mo [12], Ti–Nb [12], and Ti–Ta alloys [13]. Therefore it can be expected that Mo is the most effective β stabilizer and the β Ti–Mo alloys are more suitable than the other β Ti alloys for biomedical applications from the above viewpoint of good combination of low elastic modulus, low melting point, and low density. Up to now, Ti–15Mo [14] and Ti–7.5Mo alloys [15] have been developed for biomedical applications. However, most previous studies on Ti–Mo alloys were concentrated on the microstructures, phase transformation, and as-cast properties [4,15–25], and there are few investigations on the corrosion behavior of Ti–Mo alloys which have been subjected to thermomechanical process. On the other hand, Ti alloys often exhibit lower elastic modulus under cold deformation or solution treatment due to the presence of α″ or/and β phase [4,6,26–28], which is desirable for biomedical applications, therefore the corrosion behavior of Ti alloys including Ti–Mo alloys under such conditions should be investigated if used for biomedical applications. In this study, Ti–10Mo and Ti–20Mo (mass%) alloys cold rolled and heat treated were chosen as sample alloys for investigating their corrosion behavior to further examine their potential use in biomedical appli-

* Corresponding author. Fax: +86 757 83960006.
E-mail addresses: ylzhou@fosu.edu.cn, yinglongzhou@126.com (Y.-L. Zhou).

0925-8388/$ – see front matter © 2011 Elsevier B.V. All rights reserved.
doi:10.1016/j.jallcom.2011.03.045

Table 1
Chemical compositions of Ti–Mo alloys (mass%).

Alloy code	Mo (%)	O (%)	Ti (%)
Ti–10Mo	10.25	0.137	Bal.
Ti–20Mo	19.47	0.130	Bal.

cations. For comparative purpose, same measurements were also performed on commercial pure (CP) Ti—the currently used metallic biomaterial.

2. Experimental procedure

2.1. Material preparation

Ti–10Mo and Ti–20Mo alloys were synthesized by the following procedure. Appropriate amounts of high-purity sponge Ti (99.5 mass% purity) and Mo powder (99.8 mass% purity) were mixed. The mixtures were melted by non-consumable arc melting for three times in order to ensure chemical homogeneity. The obtained ingots were homogenized in a vacuum at 1273 K for 21.6 ks with the furnace cooling in order to eliminate the microscopic segregation of the as-cast alloys and then cold rolled (CR) into 3-mm-thick plates by the same reduction in thickness. In order to investigate the effect of cold rolling on the corrosion behavior, some samples cut from the rolled plates were subjected to a solution-treatment (ST) in a vacuum above the β-transus temperature of the alloys [16], i.e., 1123 K, for 1.8 ks, followed by their rapid quenching in ice water.

2.2. Material characterization

Microstructures of the Ti–Mo alloys were observed by scanning electron microscopy (SEM) at 20 kV. The samples for the SEM observation were ground, polished, and etched in a solution composed of 5 vol% HF, 10 vol% HNO_3, and 85 vol% H_2O. The phase constitutions of the Ti–Mo alloys were analyzed by X-ray diffraction (XRD) analysis using Cu-Kα radiation in the typical 2θ range of 30–80° with an accelerating voltage of 40 kV, current of 250 mA, and scanning speed of 1°/min.

2.3. Corrosion test

The corrosion resistance of the Ti–Mo alloys and CP Ti was evaluated by anodic polarization tests in 5% HCl solution at 310 K using an automatic potentiostat. A saturated calomel electrode and a platinum wire with a surface area of $1 \times 1.5\ cm^2$ were used as the reference electrode and counter electrode, respectively. Corrosion specimens (10 mm × 10 mm × 2 mm), acting as the working electrode, were embedded in glass cement and polished under running water with water-proof emery paper up to 1500 grit. After polishing, the specimens were cleaned with ethanol to remove grease and then rinsed with distilled water for three times. The acid solution was agitated and deaerated with high purity nitrogen gas at a flow rate of about 250 mL/min for 2.4 ks to reduce the oxygen content, and was replaced for each experiment. The cathodic treatment was then carried out at −0.9 V for 600 s to remove any oxide films present on the surface of each specimen. After the immersion in the same solution for 1.2 ks, the anodic polarization test was automatically started in the air at a sweep rate of 1 mV/s to 2.5 V (SCE). To prevent the intrusion of oxygen, nitrogen gas was also blown onto the surfaces of the samples during the polarization tests at a flow rate of $2 \times 10^{-7}\ m^3/s$. In the anodic tests, three specimens were used for CP Ti and each Ti–Mo alloy.

After the corrosion tests, the specimens were cleaned in ethanol and their chemical compositions were characterized by X-ray photoelectron spectroscopy (XPS) analysis, which was carried out with an Al-Kα source having an output of 150 W, and the X-ray spot size was set to 500 μm. The surfaces of specimens were sputtered by an Ar^+ ion beam for less 1 min prior to the XPS analysis to reduce the atmospheric carbon on the surfaces of samples. The binding energies were calibrated using the C 1s peak. The microstructures of surfaces exposed for the anodic testes were observed by SEM for all the samples.

3. Results

3.1. Chemical compositions of studied alloys

In order to check the actual chemical compositions of studied alloys, the Ti–10Mo and Ti–20Mo alloys were subjected to wet chemical and gas analysis. The results, which are shown in Table 1, reveal that the chemical compositions of two Ti–Mo alloys are closely related to their nominal compositions, indicating that the Ti–Mo alloys were synthesized successfully.

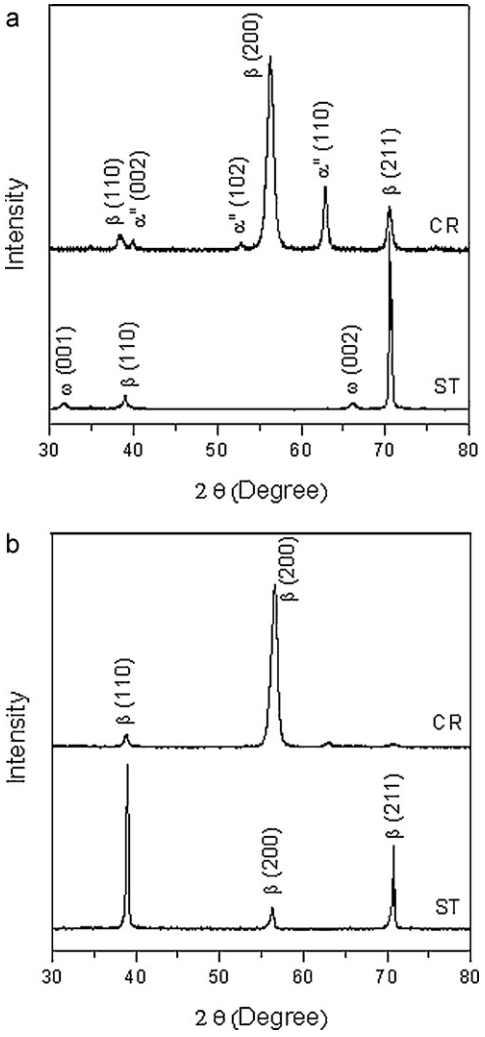

Fig. 1. XRD patterns of (a) CR + ST Ti–10Mo alloy and (b) CR + ST Ti–20Mo alloy.

3.2. Microstructural characteristics

The XRD patterns of Ti–Mo alloys are shown in Fig. 1. It can be observed that the CR Ti–10Mo alloy is composed of β + α″ two phases and the CR Ti–20Mo alloy comprises only single β phase. The CR Ti–Mo alloys exhibit obvious texture because their strongest peaks are (2 0 0) rather than (1 1 0) or (2 1 1) which is normally the strong peak of β phase [29]. After the solution treatment, however, the texture of Ti–Mo alloys disappears since the strong peaks change from (2 0 0) to (1 1 0) or (2 1 1). And new ω phase except β is detected in the ST Ti–10Mo alloy and the ST Ti–20Mo alloy is still composed of single β phase. No martensite was transformed when quenched from the β field, which indicates the Ms (martensitic start) transformation temperature is below room temperature for both of the alloys. The phase transformations after the solution treatment are in agreement with the previous studies [12,16].

It is expected that before the cold rolling, the Ti–10Mo and Ti–20Mo alloys after the homogenization heat treatment with furnace cooling should exhibit single β phase according to Refs. [4,16]. However, after the cold rolling, martensite α″ and β phases were detected in the Ti–10Mo alloy. This is related to the strain-induced martensite α″ transformation (SIMT) from β phase to martensite α″ during plastic deformation that only occurred in the Ti–10Mo alloy, which will be discussed in a separate report.

The SEM microstructures of Ti–Mo alloys are shown in Fig. 2. It can be observed that the CR Ti–Mo alloys exhibit microstruc-

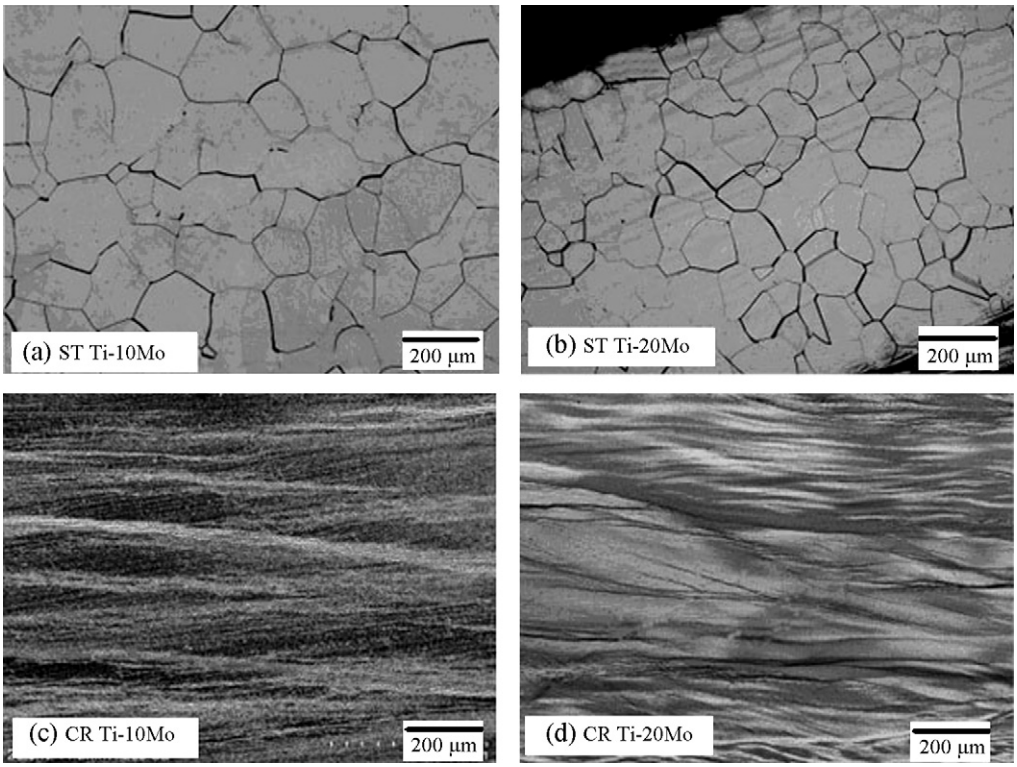

Fig. 2. SEM microstructures of Ti–Mo alloys.

tures with obvious fibrous stripe, which corresponds with the rolling texture detected by the above XRD analysis. By contrast, the ST Ti–Mo alloys exhibit similar microstructures with equiaxed β grains, which is in agreement with the above XRD results. No other significant difference exists in their microstructures except larger β grains in the ST Ti–10Mo alloy than in the ST Ti–20Mo alloy. The ω phase detected by the XRD analysis is invisible in the SEM microstructure of Ti–10Mo alloy, which may be related to its very small size and limited SEM resolution.

3.3. Corrosion characteristics

The corrosion resistance of Ti implants is improved by the formation of extremely thin and dense oxide films (passive films) over the surfaces of the implants. The passive film formation and stability are usually evaluated by anodic polarization tests. The physiological fluids are chloride solution with pH 7.4 and homeostatically maintained at 310 K (37 °C), which are much aggressive than the air or moisture environment. When the Ti alloys are implanted into human bodies, they come into contact with the body fluid containing mainly Na^+ and Cl^- [30]. To simulate these phenomena, 5% HCl solution is often chosen as a testing solution [30–33].

The anodic polarization curves of the Ti–Mo alloys and CP Ti in 5% HCl solution are shown in Fig. 3. It can be observed that all the curves are similar on the whole with obvious passive characteristics, which indicates the passive film formation on the surfaces of CP Ti and all the (CR and ST) Ti–Mo alloys. The passive current densities of the Ti–Mo alloys keep almost unchanged inside their wide passive regions, revealing that their corrosion rates are in steady state and the passive films formed on the surfaces are stable. All the Ti–Mo alloys show smaller passive current densities (i_{pc}) as compared to CP Ti, indicating that those alloys are more corrosion resistant than CP Ti. The passive current density of (CR and ST) Ti–Mo alloy gradually decreases with the Mo content, implying

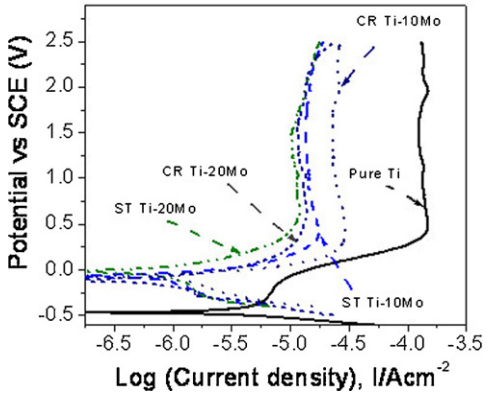

Fig. 3. Anodic curves of CP Ti and Ti–Mo alloys in 5% HCl solution at 310 K.

that the corrosion resistance of Ti–Mo alloy increases with Mo content. The passive current densities of Ti–Mo alloys in 5% HCl solution are close to those of the Ti–Ta–Nb alloys in Ringer's solution [34], and Ti–Mo alloys in Hanks' solution [15] and in fluoridated physiological serum [25], which are all less than 10 μA/cm^2, suggesting a high possibility for the Ti–Mo alloys to be passivated in a human body environment according to the previous study [15], since all the corrosive solutions belong to the similar simulated physiological media. No potential breakdown is observed up to 2.5 V for all the specimens. It also can be noticed that the corrosion potential of Ti–Mo alloy shifts in the noble direction as compared with CP Ti. This trend is similar to those observed on the additions of Hf [31], Ta [32], Mo [33], and Pt [35] to the Ti alloys, respectively. Small oscillations of current density for CP Ti are observed in Fig. 3, which is related to the consecutive formation and repassivation of microsize pits, commonly called metastable pits [25].

It also can be observed from Fig. 3 that the CR Ti–Mo alloy has bigger passive current density than the corresponding ST Ti–Mo

alloy despite the same chemical composition, which is related to the cold rolling process. It is well-known that the extra free energy, high density of dislocation, texture, and internal stress caused by the plastic deformation may accelerate the corrosion [36–39], which helps to understand that the CR Ti–20Mo alloy has bigger passive current density than the ST Ti–20Mo alloy in spite of the same Mo content and constituent phase. The CR Ti–10Mo alloy with ($\alpha'' + \beta$) phases has bigger passive current density than the ST Ti–10Mo alloy with ω plus β phases, which is associated with the effects of both cold rolling and second phase on the corrosion behavior. The difference in passive current density between the CR and ST Ti–10Mo alloys is bigger than that between the CR and ST Ti–20Mo alloys, which is related to the effects of Mo content and second phase on the corrosion behavior since the effect of same cold rolling process on the corrosion behavior of Ti–Mo alloys should be same. The detailed information on effects of ω and α'' phases on the corrosion behavior of Ti alloys is not readily available, thus deeper discussion is impossible in this study and further experiment is necessary.

The surface morphologies of CP Ti and the Ti–Mo alloys after anodic tests in 5% HCl solution are shown in Fig. 4. The oxide films formed on the surfaces of CP Ti and the Ti–Mo alloys are basically non-porous barriers (compact and uniform) characterized by grooves and ridges, except for a few of small pits over the surface of CP Ti as indicated by arrows in Fig. 4(a). Those suggest that the Ti–Mo alloys exhibit better corrosion resistance than CP Ti, which is in agreement with the above polarization data as shown in Fig. 3. There is no obvious difference in the surface morphologies between the CR and ST Ti–Mo alloys, which indicates that the extra free energy, higher density of dislocations, texture, and internal stress caused by the cold rolling had no obvious effect on the formation of passive films on the alloys although they lead to bigger passive current density of the CR Ti–Mo alloy than that of the corresponding ST Ti–Mo alloy.

The small pits over the surface of CP Ti are related to the small oscillations of current density as shown in Fig. 3, since it is well-known that the chloride solutions strongly promote the anodic dissolution of TiO_2/Ti [40–44], and pitting corrosion of pure Ti and its alloys has been often observed [25,31,32,40–43]. In the presence of chloride ions, Cl^- can migrate across the passivating oxide film in parallel with oxide ions. Thus, if Cl^- reaches the metal/film

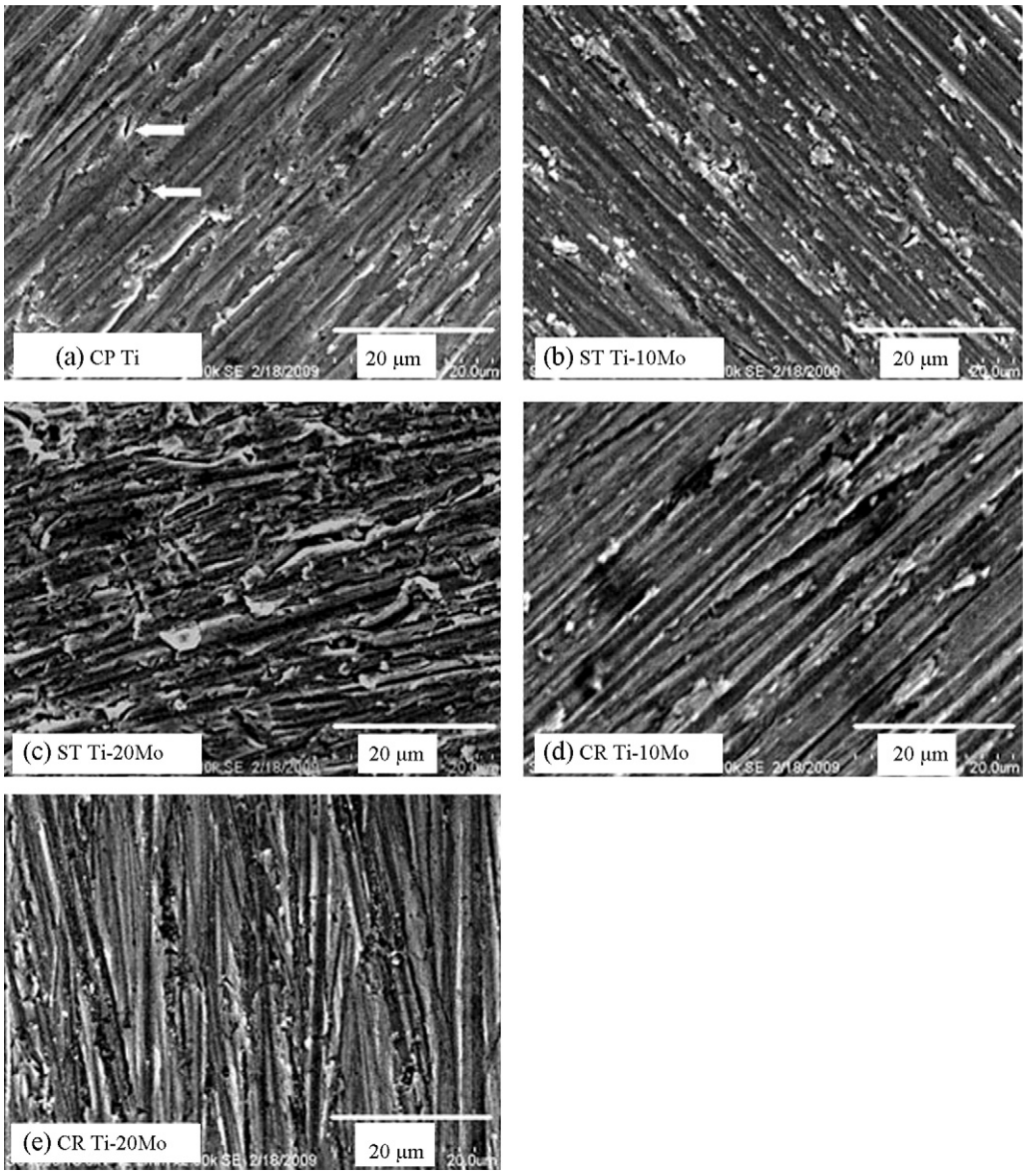

Fig. 4. The surface morphology of CP Ti and Ti–Mo alloys after anodic tests in 5% HCl solution.

interface, it would form the metal chloride. Accumulation of metal chloride (or perhaps in the case of titanium, metal oxychloride) at the metal/film interface may cause oxide film rupture, resulting in the initiation of pits [44]. The ability to propagate a metastably growing pit then depends on the amount of chloride accumulated at the nucleated site [44]. This mechanism may explain the reason why some small pits formed over the surface of CP Ti in this study.

For the characterization of passive films on the surfaces of Ti–Mo alloys and CP Ti, the specimens were cleaned in ethanol after corrosion tests and then examined by XPS analysis. Fig. 5 shows the scan-survey spectra for the passive films formed on the surface of CP Ti after anodic tests. The wide-scan survey spectrum of passive films formed on the surface of CP Ti is shown in Fig. 5(a), which confirms the presence of O, Ti, C, and N. The peaks of C 1s and N 1s observed in the wide-scan spectrum of CP Ti are attributed to the surface contamination of specimens during experiments, as shown in previous studies [31,45–47]. Fig. 5(b) shows the narrow-scan survey spectrum of oxygen. The presence of the O 1s spectrum consisted of two peaks: the primary peak located at 530.5 eV is attributed to the presence of OM oxygen (oxide oxygen) on the surface, and the minor peak at 532.5 eV corresponds to the OH oxygen [48–50]. The OM oxygen corresponds to O^{2-} ions in oxide in the surface film, and the OH oxygen is composed of OH^- ions and bound water in the surface film. The O^{2-} is more intense than the OH^- peak. Fig. 5(c) shows the narrow-scan spectrum of Ti 2p with two peaks at 458.8 eV and 464.5 eV, which correspond to Ti^{4+} oxidation state [47,50]. Therefore, the above XPS results indicate that the passive films formed on the surface of CP Ti mainly consist of the oxide film TiO_2.

The CR and ST Ti–Mo alloys exhibit similar spectra of elements, therefore only the scan-survey spectra of passive films formed on the surface of ST Ti–10Mo alloy are presented in Fig. 6. Fig. 6(a) shows the wide-scan survey spectrum of passive films formed on the surface of specimen after anodic test. From this spectrum, the presence of O, Ti, Mo, C, and N was confirmed. Fig. 6(b) and (c), similar to Fig. 5b and c, respectively, which show the narrow-scan survey spectra of O^{2-} and Ti^{4+}, respectively. Fig. 6(d) shows the narrow-scan spectrum of Mo 3d, which exhibits two peaks—one at 232.8 eV and the other at 235.5 eV. Those two peaks can be

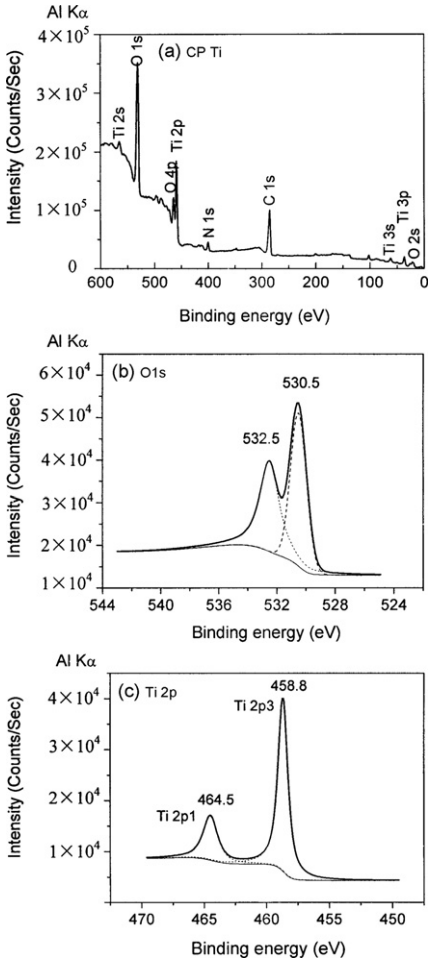

Fig. 5. Scan-survey spectra for the passive films formed on CP Ti in 5% HCl solution.

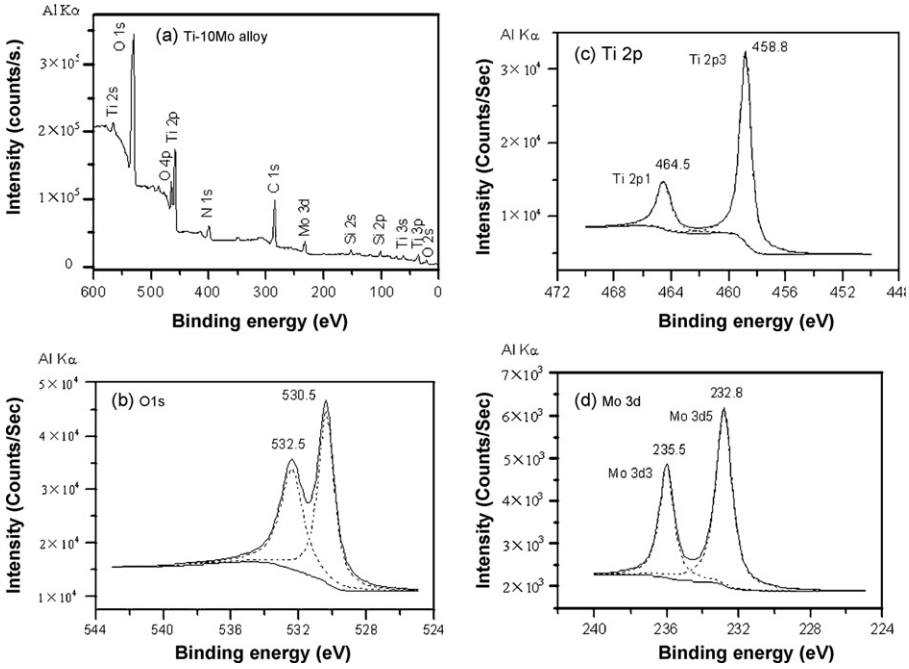

Fig. 6. Scan-survey spectra for the passive films formed on the ST Ti–10Mo alloy in 5% HCl solution.

attributed to the presence of MoO_3 formation in the films [50–52]. On combining Fig. 6(b) with Fig. 6c and d, it can be concluded that the passive films formed on the surface of Ti–10Mo alloy consist of a mixture of both TiO_2 and MoO_3, since the peaks of OM oxygen (O^{2-}) ions are the same for both the molybdenum dioxide and titanium dioxide. The intensity of the Mo 3d as shown in Fig. 6(d) is much smaller than that of Ti 2p as shown in Figs. 5(c) and 6(c), which indicates that the main component in the passive films is TiO_2 for both pure Ti and Ti–10Mo alloy. This is related to that the concentrations of element Ti are much higher than those of Mo in both CP Ti and Ti–10Mo alloy.

The high corrosion resistance of pure Ti and its alloys is due to the formation of highly stable, continuous, protective oxide films on their surfaces within milliseconds of exposure to corrosive media with a wide range of pH [21–25,30–43,53–57], which is also proved by this study. On combining the anodic polarization curves (Fig. 3) with the scan-survey spectra of passive films (Figs. 5 and 6), it can be observed that CP Ti exhibits good corrosion behavior because of the formation of protective oxide film TiO_2, and the Ti–Mo alloys exhibit good corrosion behavior due to the passive film formation of a mixture of TiO_2 and MoO_3. The stronger the passive film that forms on the surface of an implant is, the better the corrosion resistance of the implant is [45,58]. In this study, the Ti–Mo alloys exhibit better corrosion resistance than CP Ti, which suggests that the passive film of a mixture of TiO_2 and MoO_3 is more stable and stronger than the passive film TiO_2, and the Ti–Mo alloys are suitable than CP Ti for biomedical application from the viewpoint of good corrosion resistance.

4. Conclusions

In this study, the corrosion resistance of Ti–Mo alloys cold rolled and solution treated was investigated in 5% HCl solution at 310 K. The main conclusions are summarized as follows.

Both of the Ti–Mo alloys cold rolled and solution heat treated exhibit a passive behavior in 5% HCl solution, which is attributed to the passive film formation of a mixture of MoO_3 and TiO_2. The cold rolling process does not influence the formation of passive films on the Ti–Mo alloys although it slightly increases the passive current densities. The corrosion resistance of Ti–Mo alloys increases with Mo content and both of the Ti–Mo alloys exhibit better corrosion resistance than CP Ti—the currently used metallic biomaterial.

Acknowledgements

The work was financially supported by the Scientific Research Foundation for the Returned Overseas Chinese Scholars, State Education Ministry of PR China (Grant No. 2008/890). Kind help from Dr S.J. Li, Associate Professor of the Institute of Metal Research, Chinese Academy of Sciences, PR China was also acknowledged.

References

[1] M. Niinomi, Metall. Mater. Trans. 33 A (2002) 477–486.
[2] M. Niinomi, Mater. Sci. Eng. A 243 (1998) 231–236.
[3] M. Long, H.J. Rack, Biomaterials 19 (1998) 1621–1639.
[4] W.F. Ho, C.P. Ju, J.H. Chern Lin, Biomaterials 20 (1999) 2115–2122.
[5] C.M. Lee, C.P. Ju, J.H. Chern Lin, J. Oral Rehabil. 29 (2002) 314–322.
[6] Y.-L. Zhou, M. Niinomi, T. Akahori, Mater. Sci. Eng. A 371 (2004) 283–290.
[7] Y.-L. Zhou, M. Niinomi, T. Akahori, Mater. Sci. Eng. A 384 (2004) 92–101.
[8] Y.-L. Zhou, M. Niinomi, J. Alloys Compd. 466 (2008) 535–542.
[9] Y.-L. Zhou, M. Niinomi, Mater. Sci. Eng. C 29 (2009) 1061–1065.
[10] The University of Sheffield and WebElements Ltd., UK, website: http://www.webelements.com/niobium/physics.html, http://www.webelements.com/tantalum/physics.html, http://www.webelements.com/molybdenum/physics.html, 2008.
[11] G. He, J. Eckert, Q.L. Dai, M.L. Sui, W. Löser, M. Hagiwara, E. Ma, Biomaterials 24 (2003) 5115–5120.
[12] I.A. Bagariatskii, G.I. Nosova, T.V. Tagunova, Tech. Phys. (1959) 1014–1018.
[13] S.G. Fedotov, T.V. Chelidez, Y.K. Kovneristyy, V.V. Sanadze, Phys. Met. Metall. 62 (1986) 109–113.
[14] K. Wang, Mater. Sci. Eng. A 213 (1996) 134–137.
[15] W.F. Ho, J. Alloy Compd. 464 (2008) 580–583.
[16] J.L. Murry, Phase Diagram of Binary Titanium Alloys, ASM International, Metal Park, OH, 1987.
[17] R. Davis, H.M. Flower, D.R.F. West, J. Mater. Sci. 14 (1979) 712–722.
[18] T. Furuhara, T. Makino, Y. Idei, H. Ishigaki, A. Takada, T. Maki, Mater. Trans. 39 (1998) 31–39.
[19] Y.Y. Chen, L.J. Xu, Z.G. Liu, F.T. Kong, Z.Y. Chen, Trans. Nonferrous Met. Soc. China 16 (2006) s824–s828.
[20] N.T.C. Oliveira, G. Aleixo, R. Caram, A.C. Gaustaldi, Mater. Sci. Eng. A 452–453 (2007) 727–731.
[21] N.T.C. Oliveira, A.C. Gaustaldi, Corros. Sci. 50 (2008) 938–945.
[22] N.T.C. Oliveira, A.C. Gaustaldi, Acta Biomater. 5 (2009) 399–405.
[23] S. Kumar, T.S.N. Sankara Narayanan, J. Dent. 36 (2008) 500–507.
[24] M.V. Capela, H.A. Acciari, J.M.V. Capela, T.M. Carvalho, M.C.S. Melin, J. Alloy Compd. 465 (2008) 479–483.
[25] A.P.R. Alves, F.A. Santana, L.A.A. Rosa, S.A. Cursino, E.N. Codaro, Mater. Sci. Eng. C 24 (2004) 693–696.
[26] E.W. Collings, The Physical Metallurgy of Titanium Alloys, ASM, Metals Park, OH, 1984.
[27] Y.L. Hao, S.J. Li, S.Y. Sun, C.Y. Zheng, R. Yang, Acta Biomater. 3 (2007) 277–286.
[28] E.W. Robare, C.M. Bugle, J.A. Davidson, K.P. Daigle, in: I. Weiss, R. Srinivasan, P.J. Bania, D. Eylon, S.L. Semiation (Eds.), The Minerals, Metals & Materials Society, 1997, pp. 283–291.
[29] E.A. Bophcoba, Metallography of Titanium Alloys (In Russian), translated by S.Q. Chen, China Defense Industry Press, Beijing, 1986, 04.
[30] Y. Okazaki, A. Ito, T. Tateishi, Y. Ito, Mater. Trans. 35 (1994) 58–66.
[31] Y.-L. Zhou, M. Niinomi, Surf. Coat. Technol. 204 (2009) 180–186.
[32] Y.-L. Zhou, M. Niinomi, T. Akahori, H. Fukui, H. Toda, Mater. Sci. Eng. A 398 (2005) 28–36.
[33] Y. Okazaki, K. Kyo, Y. Ito, T. Tateishi, Mater. Trans. 38 (1997) 344–352.
[34] A.I. Karayan, S.W. Park, K.M. Lee, Mater. Lett. 62 (2008) 1843–1845.
[35] M. Stern, H. Wissenberg, J. Electrochem. Soc. 106 (1959) 759–764.
[36] J.R. Davis, Corrosion Understanding the Basics, ASM International, Materials Park, 2000.
[37] ASM International Handbook Committee, ASM Handbook, Corrosion, vol. 13, ASM International, 1987.
[38] L.L. Shreir, Corrosion vol. 1: Corrosion of Metals and Alloys, George Newnes Ltd., London, 1963.
[39] F.L. Laque, H.R. Copson, Corrosion Resistance of Metals and Alloys, Reinhold Publishing Corporation, Chapman & Hall Ltd., New York, London, 1963.
[40] N. Casillas, S.J. Charlebois, W.H. Smyrl, H.S. White, J. Electrochem. Soc. 140 (1993) L142–L145.
[41] S.B. Basame, H.S. White, J. Electrochem. Soc. 147 (2000) 1376–1381.
[42] N. Casillas, S. Charlebois, W.H. Smyrl, H.S. White, J. Electrochem. Soc. 141 (1994) 636–642.
[43] G.T. Burstein, R.M. Souto, Electrochim. Acta 40 (1995) 1881–1888.
[44] G.T. Burstein, C. Liu, R.M. Souto, Biomaterials 26 (2005) 245–256.
[45] Y. Okazaki, T. Tateishi, Y. Ito, Mater. Trans. 38 (1997) 78–84.
[46] Y. Tanaka, M. Nakai, T. Akahori, M. Niinomi, Y. Tsutsmi, H. Doi, T. Hanawa, Corros. Sci. 50 (2008) 2111–2116.
[47] J. Domaradzki, D. Kaczmarek, E.L. Prociow, A. Borkowska, R. Kudrawiec, J. Misiewicz, D. Schmeisser, G. Beuckert, Surf. Coat. Technol. 200 (2006) 6283–6287.
[48] Y. Wang, Z. Lin, X. Cheng, H. Xiao, F. Zhang, S. Zou, Appl. Surf. Sci. 228 (2004) 93–99.
[49] G. Cabello, L. Lillo, G.E. Buono-Core, J. Non-Cryst. Solids 354 (2008) 982–988.
[50] X-ray Photoelectron Spectroscopy Database 20, Version 3.4, National Institute of Standards and Technology (NIST).
[51] Z. Li, L. Gao, S. Zheng, Appl. Catal. A: Gen. 236 (2002) 163–171.
[52] T.G.S. Cruz, A. Gorenstein, R. Landers, G.G. Kleiman, S.C. deCastro, J. Electron. Spectrosc. Relat. Phenom. 101–103 (1999) 397–400.
[53] M. Levy, G.N. Sklover, J. Electrochem. Soc. 116 (1969) 323–328.
[54] D.D.N. Singh, J. Electrochem. Soc. 132 (1985) 378–381.
[55] D.G. Kolman, J.R. Scully, J. Electrochem. Soc. 141 (1994) 2633–2641.
[56] D.F. Taylor, Encyclopedia of Chemical Technology, vol. 19, 2nd ed., John Wiley & Sons, 1969, pp. 630–652.
[57] C.E.B. Marino, E.M. de Oliveira, R.C. Rocha-Filho, S.R. Biaggio, Corros. Sci. 43 (2001) 1465–1476.
[58] Y. Okazaki, Biomaterials 23 (2002) 2071–2077.